Acoustic Vibration of Metal Films and Nanoparticles

N. Del Fatti, C. Voisin, D. Christofilos, F. Vallée,* and C. Flytzanis

Laboratoire d'Optique Quantique du CNRS, Ecole Polytechnique, 91128 Palaiseau Cedex, France

Received: November 16, 1999; In Final Form: January 27, 2000

Acoustic vibration of silver films and nanoparticles in glass, due to impulsive excitation of their fundamental expansion mode, is investigated using a femtosecond pump−probe technique. The vibrational motion is monitored via the induced modulation of the material optical properties which, in the two systems, is shown to reflect that of the real part of the dielectric function. The observed differences in their time responses are attributed to the strong coupling of the nanoparticles with their glass environment. In both systems, the phase and the amplitude of the observed oscillations are in quantitative agreement with an indirect displacive excitation process associated with lattice expansion. Control of the acoustic vibration by two femtosecond pulses is also discussed.

I. Introduction

Finite size elastic bodies exhibit vibrational normal modes associated with changes of their shape or volume. These morphological resonances usually appear at very low frequencies and have little impact on the intrinsic system properties. This is not the case for nanometric size objects where they are a manifestation of the confinement of the long wavelength acoustic vibrations and, for not too small objects, can be described using either a macroscopic (elastic body) or a microscopic (atomistic) approach.[1−4] In metallic systems, this alteration of the confined material phonon spectrum as compared to the bulk one leads, for instance, to size-dependent heat capacity and electron−lattice interactions.[2,5−8] Information on the confined mode characteristics is thus of central interest for the understanding of the specific properties of nanoscopic materials.

Time-resolved techniques have been recently applied to the investigation of the low frequency vibrational modes of semiconductor[9,10] and metal[11−14] nanocrystallites. In contrast to Raman measurements,[15] the nanoparticle fundamental radial (breathing) mode is selectively observed, permitting determination of both its frequency and, for the first time, its damping.[10,13,14] Pump−probe type of experiments were used where in-phase acoustic vibration of the nanoparticles is launched after electron excitation by a femtosecond pump pulse and detected via the induced modulation of the sample absorption of a femtosecond probe pulse. In this paper we discuss the physical origin of this modulation and of the acoustic mode excitation in metal nanocrystallites by comparing measurements performed in silver nanoparticles embedded in a glass matrix and in optically thin silver films on a substrate. In both systems, breathing mode oscillations are observed and the results are interpreted in terms of induced changes of the metal dielectric function in the confined and bulk-like systems.

II. Optical Properties

The optical properties of metallic systems are related to both the conduction and bound electron responses. In noble metals, the conduction electrons follow a quasi-free-electron behavior and their contribution to the dielectric constant is well described by the Drude formula.[16] The bulk material dielectric constant $\epsilon = \epsilon_1 + i\epsilon_2$ at the frequency ω can thus be written

$$\epsilon(\omega) = \epsilon^b(\omega) - \frac{\omega_p^2}{\omega(\omega + i\gamma_f)} \tag{1}$$

where $\omega_p = (n_e e^2/\epsilon_0 m_e)^{1/2}$ is the bulk plasmon frequency, n_e and m_e the conduction electron density and effective mass, respectively, and γ_f the quasi-free-electron optical scattering rate. The bound electron term $\epsilon^b(\omega)$ is dominated in noble metals by the interband transitions from the fully occupied d-bands below the Fermi energy to the half filled s−p conduction band.

In our experiments, we are interested in the changes $\Delta\epsilon$ of the dielectric function induced by selective energy injection in the conduction electrons and by the subsequent lattice heating as the system thermalizes. Both the interband and intraband contributions to ϵ are modified and $\Delta\epsilon_1$ can be written

$$\Delta\epsilon_1(\omega) \approx \Delta\epsilon_1^b(\omega) - \frac{2\omega_p}{\omega^2}\Delta\omega_p \tag{2}$$

(for weak damping ($\gamma_f \ll \omega$) the $\Delta\gamma_f$ contribution is negligible). Rise of the electron temperature essentially leads to a change of the interband part of ϵ which thus dominates the short time scale response.[17] Lattice heating and the concomitant lattice expansion induce electronic band displacement and warping.[18,19] This can alter both the interband term, via the energy band shift, and the intraband one, via plasmon frequency change due to reduction of the density n_e and alteration of the effective mass m_e. The lattice heat capacity being much larger than the electronic one, the temperature rise of the thermalized system is small and, on a long time scale, the main contributions to $\Delta\epsilon_1$ are related to the lattice heating.

For frequencies below the threshold for interband absorption ($\hbar\Omega_{ib} \approx 4.1$ eV) $\Delta\epsilon_2^b \approx 0$ and the change of the imaginary part of the dielectric function essentially depends on $\Delta\gamma_f$

* Corresponding author.

10.1021/jp994051y CCC: $19.00
Published on Web 03/28/2000

$$\Delta\epsilon_2(\omega) \approx \frac{\omega_p^2}{\omega^3}\Delta\gamma_f \tag{3}$$

and has thus a different physical origin than $\Delta\epsilon_1$ (the $\Delta\omega_p$ contribution is here negligible). At room temperature γ_f is determined by electron−phonon scattering and is almost proportional to the lattice temperature T_L. Consequently, $\Delta\gamma$ essentially reflects the T_L rise.

The above description is a priori valid only for a bulk material but can be generalized to the case of nanocrystallites. For not too small particles (typically with radius $R \geq 1.5$ nm), quantum confinement effects lead only to small modifications of the band structure (the interband transitions are in particular not significantly modified[20]) and a similar form of the metal dielectric function in the nanocrystals can be used by replacing γ_f with

$$\gamma = \gamma_f + g_S\frac{v_F}{R} \tag{4}$$

where v_F is the Fermi velocity and g_S a constant.[21] Using a classical description, this additional term reflects the new diffusion process due to electron scattering off the surfaces.

In usual experiments, the optical properties of a composite material, formed by an ensemble of metal nanoparticles dispersed in a transparent matrix is investigated. They also depend on the matrix dielectric constant ϵ_d which is assumed real and undispersed. For a low volume fraction $p \ll 1$ of small spherical nanocrystals, $R \ll \lambda$, where λ is the optical wavelength, one can show that the material absorption coefficient is related to ϵ by[21]

$$\tilde{\alpha}(\omega) = \frac{9p\epsilon_d^{3/2}}{c}\frac{\omega\epsilon_2(\omega)}{[\epsilon_1(\omega)+2\epsilon_d]^2+\epsilon_2^2(\omega)} \tag{5}$$

It is resonantly enhanced by dielectric confinement, around the frequency, Ω_R, minimizing the denominator which is the condition for the surface plasmon resonance (SPR). If ϵ_2 is weakly dispersed, Ω_R is determined by the condition

$$\epsilon_1(\Omega_R) + 2\epsilon_d = 0 \tag{6}$$

and thus essentially depends on the real part of the metal crystallite dielectric function.

The SPR line shape takes a simple quasi-Lorentzian form if ϵ_1^b is weakly dispersed (i.e., $(\partial\epsilon_1^b/\partial\omega)_{\Omega_R} \ll 2\omega_p^2/\Omega_R^3$)

$$\tilde{\alpha}(\omega) = \frac{A\omega^2\Omega_R^4\,\gamma}{(\omega^2-\Omega_R^2)^2+(\Omega_R^2\,\gamma/\omega)^2} \tag{7}$$

where A is a constant and $\Omega_R \approx \omega_p/\sqrt{\epsilon_1^b+2\epsilon_d}$. This approximation can be performed in the case of silver where the SPR is far from the interband transition threshold ($\hbar\Omega_R \approx 2.93$ eV, Figure 1) and the experimental absorption spectrum is very well reproduced by eq 7 (Figure 1).

As in bulk metal, heating of the conduction electrons and of the lattice leads to modification of the nanocrystallite dielectric function. The composite material absorption being enhanced in the vicinity of the SPR, large modifications of its optical properties can be induced and detected, permitting precise investigation of the ϵ change dynamics and its comparison with that in metal films.

III. Experimental Technique

Experiments were performed at room temperature in $R = 13$ nm spherical silver nanoparticles embedded in a

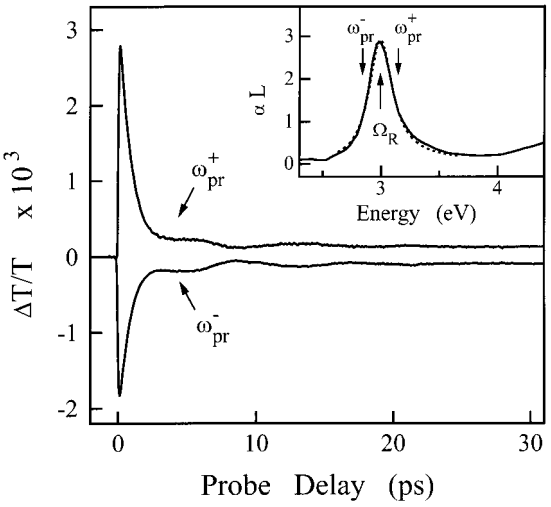

Figure 1. Transmission change $\Delta T/T$ in $R = 13$ nm Ag nanoparticles in a glass matrix for two probe photon energies $\hbar\omega_{pr}^+ = 3$ eV and $\hbar\omega_{pr}^- = 2.85$ eV around the surface plasmon resonance frequency $\hbar\Omega_R = 2.93$ eV. The pump fluence is 0.1 mJ/cm^2. The inset shows the sample absorption spectrum around $\hbar\Omega_R$. The probing frequencies are schematically indicated by the arrows.

$50BaO\text{-}50P_2O_5$ glass matrix[22] and in optically thin silver films on a sapphire substrate, using either a one- or a two-color femtosecond pump−probe technique. In both systems, energy is first injected in the electron gas by intraband (free electron) absorption of an 80 fs near-infrared pulse delivered by a frequency tunable Ti:sapphire oscillator. Measurements were performed in the low perturbation regime with a maximum transient rise of the electron temperature of less than 100 K, corresponding to a final temperature rise of less than 1 K for the thermalized electron−lattice system.

In the nanoparticle sample, the time-dependent induced transmission change $\Delta T/T$ is probed around the SPR frequency using a 100 fs blue pulse, $\hbar\omega_{pr}$, created by frequency doubling part of the pulse train in a 1 mm thick BBO crystal. In our samples the induced reflectivity changes are negligible and $\Delta T/T$ thus directly reflects the absorption change: $\Delta T/T(\omega_{pr}) = -\Delta\alpha(\omega_{pr})L$ where L is the sample thickness ($\sim$15 μm).

In thin films, the induced reflectivity, $\Delta R/R$, and transmissivity, $\Delta T/T$, changes were measured either in the infrared, at the same wavelength as the pump pulse, or in the blue, at the double frequency. In the perturbative regime, $\Delta T/T$ and $\Delta R/R$ are linear combinations of the changes of the real and imaginary parts of the dielectric function

$$\begin{aligned}\Delta T/T(\omega_{pr}) &= t_1\Delta\epsilon_1(\omega_{pr}) + t_2\Delta\epsilon_2(\omega_{pr})\\ \Delta R/R(\omega_{pr}) &= r_1\Delta\epsilon_1(\omega_{pr}) + r_2\Delta\epsilon_2(\omega_{pr})\end{aligned} \tag{8}$$

that can thus be extracted (the ω_{pr}-dependent coefficients t_1, t_2, r_1, and r_2 are computed from the equilibrium dielectric function measured in metal films, taking into account the Fabry−Perot effect[16,23]).

In both cases, a standard pump−probe setup has been used with mechanical chopping of the pump beam at 1.5 kHz and lock-in detection of the transmitted or reflected probe beam. The size of the focal spots were measured to be $\sim$30 μm in diameter. The zero delay was measured by cross-correlation of the pump and probe pulses in a 100 μm thick BBO crystal. The high repetition rate (80 MHz) and good stability of our femtosecond system permits noise levels for $\Delta T/T$ and $\Delta R/R$ measurements in the 10^{-6} range.

IV. Results and Discussion

A. Silver Nanoparticles. The time behavior of the differential transmission change $\Delta T/T$ measured in the $R = 13$ nm nanoparticle sample is shown in Figure 1 for two probe frequencies on the low, ω_{pr}^{-}, and high, ω_{pr}^{+}, frequency sides of Ω_R. The short time delay signals ($t \leq 3$ ps) are dominated by the conduction electron dynamics and have been discussed in detail elsewhere.[24] For both probe wavelengths, $\Delta T/T$ rises with energy injection in the electron gas and subsequently decays exponentially as energy is transferred to the lattice. The observed decay time constant $\tau_{e-ph} \approx 850$ fs is consistent with investigations in metal films.[17,25]

On a longer time scale, $\Delta T/T$ exhibits oscillations superimposed on a slowly decaying background. This background signal is a consequence of the induced temperature rise of the thermalized system and it decays on a few hundred picosecond time scale with heat diffusion to the matrix. The oscillations appear as a modulation of this background and are out of phase when probing on different sides of the SPR (i.e., when $\Delta T/T$ increases for probing at $\hbar\omega_{pr}^{-}$ it decreases at $\hbar\omega_{pr}^{+}$), showing that the observed signal is due to modulation of the SPR frequency.

The origin of the observed optical property modulation has been confirmed by performing systematic measurements as a function of $\hbar\omega_{pr}$ around the SPR.[13] The $\hbar\omega_{pr}$ dependence of $\Delta T/T$ for a fixed pump−probe delay can be very well reproduced as the difference between two quasi-Lorentzian lines (eq 7) with different frequency and width (Figure 2). The deduced shift $\Delta\Omega_R$ and broadening $\Delta\gamma$ are shown in Figure 2. Only $\Delta\Omega_R$ oscillates on a picosecond time scale while $\Delta\gamma$ reaches an almost constant positive value reflecting the increase of the electron−phonon scattering rate due to the lattice temperature rise. The $\Delta\Omega_R$ time behavior is identical to that of the measured $\Delta T/T$ for $\hbar\omega_{pr} = 2.85$ eV. It will thus be used in the following as a reference signal to analyze the Ω_R modulation.

The oscillation period, $T_{osc} \approx 8.1$ ps, is in very good agreement with the calculated one for the fundamental radial mode of $R = 13$ nm spherical nanoparticles (≈ 8 ps).[13] This mode corresponds to a simple mechanical movement of the sphere where it periodically expands and contracts (breathing mode). It is actually also associated to a movement of the surrounding glass matrix with which the spheres are strongly coupled, which, in particular, is at the origin of their damping.[3,13] The SPR frequency oscillation thus reflects the modulation of the composite material absorption due to in-phase breathing mode oscillation of the individual nanocrystallites (see section IV C). This reflects the fact that the electronic properties of each nanosphere adiabatically follow their periodic lattice property changes.

Using eqs 6 and 1, one can show that $\Delta\Omega_R$ is proportional to $\Delta\epsilon_1$

$$\Delta\Omega_R = -\frac{\Delta\epsilon_1(\Omega_R)}{(\partial\epsilon_1/\partial\omega)_{\Omega_R}} \approx -\frac{\Omega_R^3}{2\omega_p^2}\Delta\epsilon_1(\Omega_R) \qquad (9)$$

where $\Delta\epsilon_1$ is given by eq 2. The observed oscillations are thus due to that of $\Delta\epsilon_1$ and can be ascribed to modulation of the interband term and/or the intraband one (via the plasmon frequency) by the breathing mode of the particles (eq 2). Both effects can contribute to the observed modulation in nanoparticles and cannot be separated here.

Similar coherent oscillations were recently reported in gold colloids.[12,27] Probing below the SPR frequency, a similar short time delay $\Delta T/T$ has been observed as that measured in our silver sample for probing at $\hbar\omega_{pr}^{-}$ (Figure 1). In contrast, a positive $\Delta T/T$ background has, however, been observed, indicating a blue shift of the SPR on a picosecond scale, with oscillations out of phase as compared to our results (i.e., $\Delta T/T$ exhibits a maximum for a probe delay $t \approx T_{osc}/2$ in gold colloids while we observe a minimum (Figure 1)). As in both systems, the long delay signal can be correlated to the particle volume increase; the different sign of their response suggests that reduction of the electron density n_e (and thus of ω_p) plays a minor role.

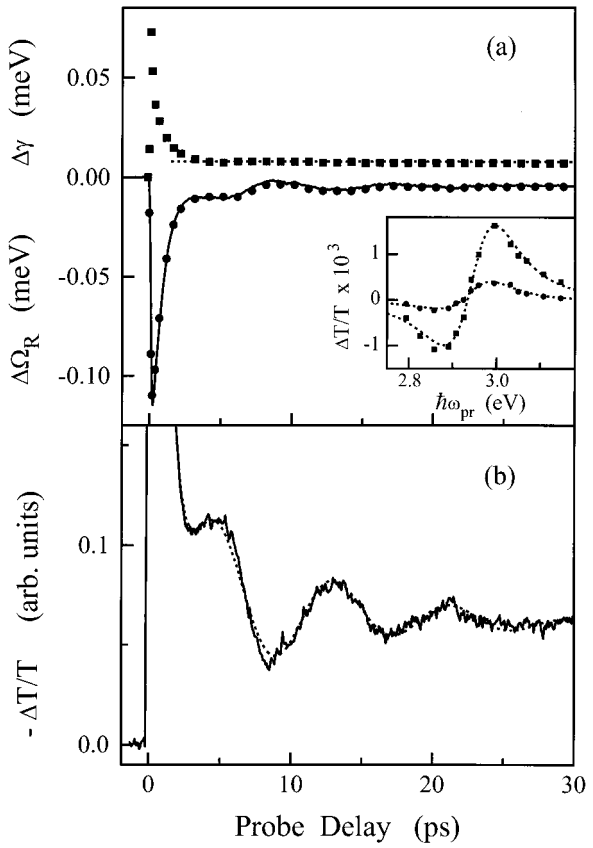

Figure 2. (a) Measured time dependence of the SPR frequency shift $\Delta\Omega_R$ (circles) and broadening $\Delta\gamma$ (squares) in $R = 13$ nm Ag nanoparticles. The full line is the normalized $\Delta T/T$ for $\hbar\omega_{pr}^{-} = 2.85$ eV, and the straight dashed line a guide to the eye. Inset: Measured $\Delta T/T$ around the SPR for probe delays of 600 fs (squares) and 3 ps (circles). The dotted lines are fits assuming a frequency shift and a broadening of the SPR. (b) Transmission change $-\Delta T/T \propto \Delta\epsilon_1$ on an enlarged scale. The dashed line is calculated for a lattice mediated displacive excitation (eq 11).

B. Silver Films. The transient transmission and reflectivity changes measured in the 23 nm thick polycrystalline silver film are shown in Figure 3 for a probe pulse in the infrared ($\hbar\omega_{pr} = 1.45$ eV). A similar behavior as that reported for silver nanoparticles is observed with a short time scale signal exponential decay (with $\tau_{e-ph} \approx 850$ fs) and oscillations superimposed on a background on a picosecond time scale (inset of Figure 3). Their measured period $T_{osc} \approx 12.3$ ps is consistent with the expansion and contraction mode of a 23 nm thick film.[26] This dilation mode is the one-dimensional analogue of the sphere breathing mode observed in nanoparticles.

The associated changes of $\Delta\epsilon_1$ and $\Delta\epsilon_2$ of the metal dielectric function can be extracted using eq 8 and are shown in Figure 3. Their short time dynamics has been discussed elsewhere[17] and we will focus here on their long delay behavior. On this

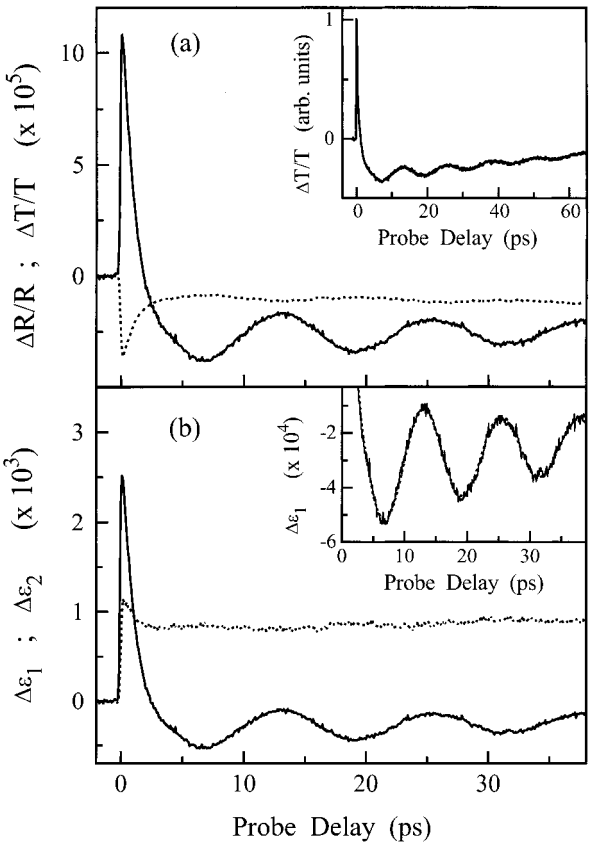

Figure 3. (a) Transient transmission $\Delta T/T$ (full line) and reflectivity $\Delta R/R$ (dashed line) changes measured in a 23 nm silver film for a near-infrared probe ($\hbar\omega_{pr} = 1.45$ eV). The pump fluence is 0.15 mJ/cm^2. The inset shows $\Delta T/T$ on a longer time scale. (b) Deduced change of the real $\Delta\epsilon_1$ (full line) and imaginary $\Delta\epsilon_2$ (dashed line) part of the dielectric function. The inset shows the long time scale behavior of $\Delta\epsilon_1$ on an enlarged scale (full line) together with a fit using eq 11 (dotted line).

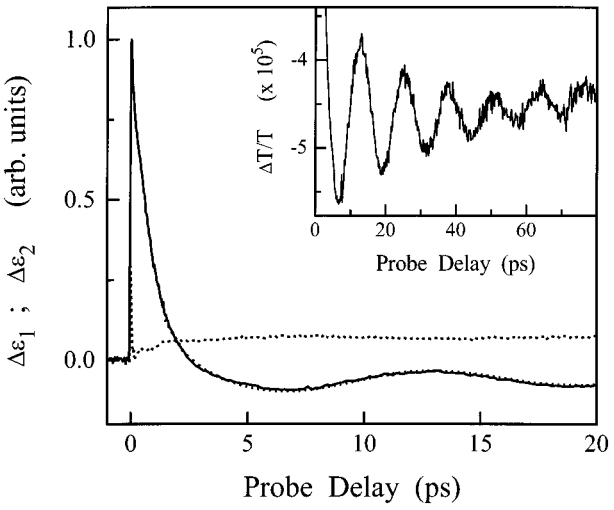

Figure 4. Measured transient changes of the real $\Delta\epsilon_1$ (full line) and imaginary $\Delta\epsilon_2$ (dashed line) part of the dielectric function in a 23 nm silver film for a probe photon energy $\hbar\omega_{pr} = 2.95$ eV. The dotted line is a fit to $\Delta\epsilon_1$ using eq 11. The inset shows the long time scale behavior of the corresponding $\Delta T/T$ (full line) on an enlarged scale.

time scale, only $\Delta\epsilon_1$ is found to oscillate while $\Delta\epsilon_2$ reaches an almost constant value which is determined by the increase of the average electron scattering rate due to the lattice temperature rise (eq 3 with $\Delta T_L \approx 0.6$ K yielding $\Delta\epsilon_2 \approx 9 \times 10^{-4}$,[17] in quantitative agreement with the measured value). The different long time behaviors of the observed $\Delta\epsilon_1$ and $\Delta\epsilon_2$ are consistent with their different physical origins discussed in section II. As in nanoparticles, the observed modulation of the film optical properties can thus be ascribed to modulation of $\Delta\epsilon_1$ by its acoustic vibration.

The rise of the metal film temperature is at the origin of the negative background value of $\Delta\epsilon_1$. This decrease of ϵ_1 with increasing T_L is in agreement with CW measurements and has been attributed to reduction of the electron effective mass (leading to $\Delta\omega_p > 0$ in eq 2).[28] Following this interpretation, the observed modulation of the film optical properties can thus be ascribed to modulation of the intraband part of ϵ_1 due to that of the electron effective mass. The same $\Delta\epsilon_1$ sign is observed probing in the blue region of the spectrum, with however smaller background and oscillation amplitudes and a reduced ϵ_2 change (Figure 4), consistent with reduction of the intraband contribution with increasing ω (eqs 2 and 3).

The observed background sign and oscillation phase are in contrast to that measured in nanoparticles where $\Delta\epsilon_1 \propto -\Delta\Omega_R > 0$ (Figure 2). A possible explanation for these different behaviors is that the thermal lattice expansion and the concomitant induced strains are largely modified in the metal nanoparticles by their glass environment as compared to the film case, leading to different relative contributions to $\Delta\epsilon_1$. This qualitative explanation is corroborated by $\Delta T/T$ measurements performed in gold colloids,[12,27] which correspond to a softer environment of the particles, where the same background sign and oscillation phase as observed in our silver film is suggested. Additional experimental, in particular as a function of the matrix, and theoretical investigations are however necessary to clarify the physical origin of these different behaviors.

C. Coherent Excitation Mechanism. In both systems, the establishment of a new quasi-equilibrium situation after ultrafast heating by the femtosecond pump pulse is concomitant with a lattice expansion. Although energy is selectively injected in the conduction electrons, it is quickly transferred to the lattice, on a time scale of the order of $\tau_{e-ph} < 1$ ps. Lattice heating is thus much faster than the expansion characteristic time (i.e., the period of the breathing mode) and the system size (nanoparticle radius or film thickness) stays almost unchanged during the heating process. It is thus smaller than the new equilibrium size imposed by the temperature rise and thus subsequently increases and starts oscillating around this new equilibrium position. This corresponds to impulsive launching of the characteristic expansion mode with a well-defined phase and an amplitude related to the equilibrium position displacement (i.e., the observed background amplitude).

A more quantitative analysis can be performed describing the observed modes by a damped harmonic oscillator model excited by displacement of its equilibrium position.[13] The response is the solution of

$$\ddot{x} + 2\frac{\dot{x}}{\tau_0} + \omega_0^2\{x - x_0[1 - \exp(-t/\tau_{e-ph})]\} = 0 \quad (10)$$

where ω_0 and τ_0 are the breathing mode frequency and effective damping time, respectively,[29] and x_0 is the new equilibrium position which is reached as the lattice heats up. With the initial conditions $x = 0$ and $\dot{x} = 0$, the solution can be written

$$x(t) = x_0 - \frac{x_0}{\sqrt{1 + (\omega_0 \tau_{e-ph})^2}} \exp(-t/\tau_0) \cos(\omega_0 t - \varphi) - \frac{x_0}{1 + (\omega_0 \tau_{e-ph})^{-2}} \exp(-t/\tau_{e-ph}) \quad (11)$$

The last term decays on an ~1 ps time scale and thus influences only the short time nonoscillating response (Figures 2−4). The two first correspond, respectively, to the linked amplitudes of the quasi-equilibrium (background) response and of the oscillations and are the contributions of interest here. The phase of the oscillations φ is given by

$$\varphi = \arctan\left(\frac{1}{\omega_0 \tau_0} + \frac{\omega_0}{1/\tau_{e-ph} - 2/\tau_0}\right) \approx \arctan(\omega_0 \tau_{e-ph}), \quad (12)$$

As the relative oscillation amplitude, the phase depends essentially on the oscillation frequency, ω_0, and on τ_{e-ph} which are precisely determined experimentally. This model describes only the lattice related response and does not include the short time scale contribution to the measured signal due to the nonequilibrium electrons. This decays exponentially with the electron temperature and can be included by adding to the lattice contribution (eq 11) a term of the form

$$S_e = B \exp(-t/\tau_{e-ph}) \quad (13)$$

where B is a fitting parameter. This, however, contributes only for $t \leq 2$ ps and does not influence the oscillating part of the signal.

As discussed above, lattice expansion leads to an increase of ϵ_1 in the nanoparticle system and a decrease in the film. $\Delta\epsilon_1$ has thus to be taken proportionally to, respectively, x and $-x$, which introduces a π phase shift for the oscillations in the two systems, as observed experimentally. Using this model, a very good description of the observed oscillation and background amplitudes is obtained in both the nanoparticle system (Figure 2) and the film (Figures 3 and 4).[30]

In both systems, the measured phase of the oscillations is also identical to that predicted by eq 12, with a quasi-cosine behavior, confirming the validity of our description. It is also consistent with the observed signal in gold colloids,[12,27] where as in the film $\Delta\epsilon_1 \propto -x$ has to be used.

In this model, we have considered only acoustic mode launching due to the indirect lattice heating by the pump pulse and to the concomitant expansion consequence of the lattice anharmonicity. In addition to this indirect displacive excitation mechanism, a direct one due to coupling with the nonequilibrium conduction electrons might also play a role. This corresponds to the application of a transient force (decaying with τ_{e-ph}) on the oscillator and thus leads to a sine type of response[14] (a similar phase is obtained for direct coupling of the mode with the pump pulse). It is in contrast to the measured phase (cosine type, i.e., with an extremum around $t = 0$), showing that it is negligible for the relatively large size systems investigated here.

V. Control of the Acoustic Motion

Inhomogeneous spatial excitation in the pump beam propagation direction has been invoked as a possible launching mechanism in gallium and tin nanoparticles,[11] in analogy with generation of coherent acoustic pulses via ultrafast electron excitation in thick metal films.[31,32] To test its possible influence, we have performed experiments exciting the nanoparticle or film samples with two synchronized counter-propagating pump pulses to reduce the excitation inhomogeneity. In both cases, the observed signal, and, in particular, the oscillation amplitude, has been found to be proportional to the total pump intensity (as for one beam excitation), demonstrating that this process is negligible here (Figures 5 and 6).

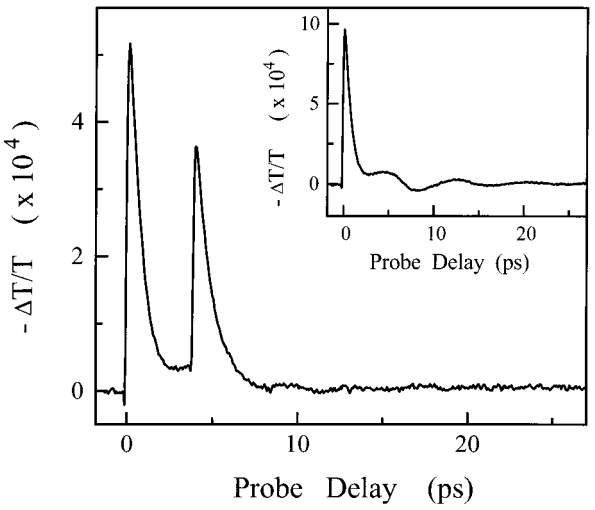

Figure 5. Transient transmission change $\Delta T/T$ induced by two counterpropagating near-infrared pump pulses delayed by half the breathing mode period ($\Delta t_{pump} = T_{osc}/2$) in R =13 nm Ag nanoparticles. The probe photon energy is $\hbar\omega_{pr} = 2.85$ eV. The inset shows $\Delta T/T$ for two synchronized counterpropagating pump pulses ($\Delta t_{pump} = 0$).

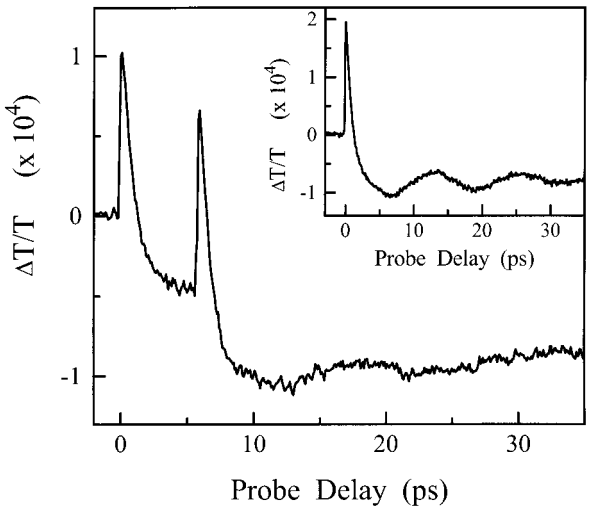

Figure 6. Transient transmission change $\Delta T/T$ induced by two counterpropagating near-infrared pump pulses delayed by half the breathing mode period ($\Delta t_{pump} = T_{osc}/2$) in the 23 nm thick silver film. The probe photon energy is $\hbar\omega_{pr} = 1.45$ eV. The inset shows $\Delta T/T$ for two synchronized counterpropagating pump pulses ($\Delta t_{pump} = 0$).

In our experiments, the expansion of the nanoparticles or of the film is impulsively launched by a femtosecond pulse. Using a multiple pump-beam configuration, it is possible to control their mechanical movement. The simplest example is its launching and stopping by two pump-pulses delayed by half the oscillation period: $\Delta t_{pump} = T_{osc}/2$. This is shown in Figure 5 for the nanoparticle sample and in Figure 6 for the film. In these experiments, the metallic systems first expand due to excitation by the first pump pulse and reach their maximum size, overshooting their new equilibrium position, after a delay of about $T_{osc}/2$. The second pump pulse then induces an ultrafast additional shift of the equilibrium size which, for proper adjustment of the pump energy, is identical to the actual size of the system at $T_{osc}/2$. As the surface expansion velocity is

zero for this delay, a new equilibrium situation is reached and the volume oscillation stops.

VI. Conclusion

Impulsive excitation of the fundamental breathing mode of silver nanoparticles in a glass matrix and of the corresponding expansion mode of an optically thin silver film has been performed using a femtosecond pulse. In both materials, energy is first injected in the conduction electrons and is transferred to the lattice with a characteristic time $\leq$ 1 ps, much faster than the period of the investigated modes. Impulsive launching of the acoustic vibration is ascribed to the concomitant lattice expansion corresponding to ultrafast displacement of the system equilibrium size (radius or thickness) which subsequently oscillates around its new equilibrium value. The oscillations are thus connected to the lattice expansion dynamics and, as observed experimentally, their amplitude and sign are correlated with those of the long-term response due to lattice expansion of the quasi-equilibrium thermalized system. Using this approach and modeling the breathing mode by a harmonic oscillator, quantitative descriptions of the observed phase and amplitude of the oscillations are obtained in both the nanoparticle system and the film. Optical control of the lattice expansion is also demonstrated using two time-delayed pump pulses.

The electronic properties of the metallic systems adiabatically follow the volume oscillation, permitting its real-time detection via the concomitant modulations of the optical properties. In both materials, they have been shown to be due to modulation of the real part of the dielectric function and have been ascribed to changes of the metal electronic band structure induced by the lattice movement. In the composite materials, this corresponds to a modulation of the electronic absorption resonance of each nanoparticle whose frequency follows its lattice changes. Although an ensemble of randomly spatially distributed metal nanoparticles is investigated, a nonzero average signal can be measured as they are mechanically moving in phase, inducing identical electronic property modulation in each particle.

Acknowledgment. The authors thank A. Nakamura and B. Perrin for helpful discussions and G. V. Hartland for communicating us his results before publication. We are also indebted to S. Omit for providing the silver nanoparticle samples.

References and Notes

(1) Satô, Y.; Usami, T. *Geophys. Magn.* **1962**, *31*, 15.
(2) Tamura, A.; Higeta, K.; Ichinokawa, T. *J. Phys. C* **1982**, *15*, 4975.
(3) Dubrovskiy, V. A.; Morochnik, V. S. *Earth Phys.* **1981**, *17*, 494.
(4) Fu, H.; Ozolins, V.; Zunger, A. *Phys. Rev. B* **1999**, *59*, 2881.
(5) Johnson, K.; Wybourne, M. N.; Perrin, N. *Phys. Rev. B* **1994**, *50*, 2035.
(6) Nisoli, M.; Stagira, S.; De Silvestri, S.; Stella, A.; Tognini, P.; Cheyssac P.; Kofman, R. *Phys. Rev. Lett.* **1997**, *78*, 3575.
(7) Zhang, J. Z. *Acc. Chem. Res.* **1997**, *30*, 423 and references therein.
(8) Averitt, R. D.; Westcott, S. L.; Hallas, N. J. *Phys. Rev. B* **1998**, *58*, R10203.
(9) Krauss, T. D.; Wise, F. W. *Phys. Rev. Lett.* **1997**, *79*, 5102.
(10) Thoen, E. R.; Steinmeyer, G.; Langlois, P.; Ippen, E. P.; Tudury, G. E.; Brito Cruz, C. H.; Barbosa, L. C.; Cesar, C. L. *Appl. Phys. Lett.* **1998**, *73*, 2149.
(11) Nisoli, M.; De Silvestri, S.; Cavalleri, A.; Malvezzi, A. M.; Stella, A.; Lanzani, G.; Cheyssac, P.; Kofman, R. *Phys. Rev. B* **1997**, *55*, R13424.
(12) Hodak, J. H.; Martini, I.; Hartland, G. V. *J. Chem. Phys.* **1998**, *108*, 9210.
(13) Del Fatti, N.; Voisin, C.; Chevy, F.; Vallée, F.; Flytzanis, C. *J. Chem. Phys.* **1999**, *110*, 11484.
(14) Voisin, C.; Del Fatti, N.; Christofilos, D.; Vallée, F. *Appl. Surf. Science*, to be published.
(15) Saviot, L.; Champagnon, B.; Duval, E.; Ekimov, A. I. *Phys. Rev. B* **1998**, *57*, 341 and references therein.
(16) Johnson, P. B.; Christy, R. W. *Phys. Rev. B* **1972**, *6*, 4370.
(17) Del Fatti, N.; Bouffanais, R.; Vallée, F.; Flytzanis, C. *Phys. Rev. Lett.* **1998**, *81*, 922.
(18) Christensen, N. E.; Seraphin, B. O. *Phys. Rev. B* **1971**, *4*, 3321.
(19) Rosei, R.; Lynch, D. W. *Phys. Rev. B* **1972**, *5*, 3883.
(20) Kreibig, U. In *Handbook of Optical Properties*, Hummel, R. E., Wissmann, P., Eds.; CRC Press: New York, 1997; Vol. 2, p 145.
(21) Kreibig, U.; Vollmer, M. *Optical Properties of Metal Clusters*, Springer-Verlag: Berlin, 1995.
(22) Uchida, K.; Kaneko, S.; Omi, S.; Hata, C.; Tanji, H.; Asahara, Y.; Ikushima, A. J.; Tokisaki, T.; Nakamura, A. *J. Opt. Soc. Am. B* **1994**, *11*, 1236.
(23) Sun, C. K.; Vallée, F.; Acioli, L. H.; Ippen, E. P.; Fujimoto, J. G. *Phys. Rev. B* **1994**, *50*, 15337.
(24) Del Fatti, N.; Flytzanis, C.; Vallée, F. *Appl. Phys. B* **1999**, *68* 433.
(25) Groeneveld, R.; Sprik, R.; Lagendijk, A. *Phys. Rev. B* **1995**, *51*, 11433.
(26) Eringen, A. C.; Suhubi, E. S. *Elastodynamics − Vol. II*, Academic Press: New York, 1975.
(27) Hodak, J. H.; Henglein, A.; Hartland, G. V. *J. Chem. Phys.* **1999**, *111*, 8613.
(28) Johnson, P. B.; Christy, R. W. *Phys. Rev. B* **1975**, *11*, 1315.
(29) The sample nanoparticle size distribution should be taken into account using R dependent mode frequency and damping, and averaging the computed response (eq 11). For a narrow size distribution, a good approximation is, however, obtained using the average ω_0 value and introducing an effective damping time τ_0 phenomenologically including inhomogeneous damping due to the particle size dispersion.[13]
(30) A slow exponential decay of the background signal amplitude ($\propto x_0$) has been added, but plays a minor role on the time scale investigated in Figures 2−4.
(31) Thomsen, C.; Grahn, H. T.; Maris H. J.; Tauc, T. J. *Phys. Rev. B* **1986**, *34*, 4129.
(32) Wright, O. B. *Phys. Rev. B* **1994**, *49*, 9985.